JOURNAL OF PROPULSION AND POWER
Vol. 23, No. 6, November–December 2007

Effect of Pressure and Propellant Composition on Graphite Rocket Nozzle Erosion Rate

Ragini Acharya* and Kenneth K. Kuo†
The Pennsylvania State University, University Park, Pennsylvania 16802

DOI: 10.2514/1.24011

The objective of this work is to study the nozzle erosion rates at a broad range of pressures from 7 to 55 MPa with two baseline propellants: one is a nonmetallized propellant and the other is a metallized propellant, called propellants S and M, respectively. A comprehensive model for graphite nozzle erosion minimization and a numerical code has been advanced to predict the nozzle throat recession rates at high pressures. Four different kinetic schemes for heterogeneous graphite oxidation reactions were compared. The recession rate was found to increase almost linearly with pressure. The magnitudes of recession rates depend on the chemical kinetic scheme and the propellant composition. Contrary to popular belief, at lower pressures ($P < 14$ MPa), the heterogeneous kinetic rates showed a pronounced effect on the erosion rates, though at higher pressures, the nozzle throat erosion is mainly diffusion controlled. This observation stresses the importance of more accurate and definitive kinetic parameters for graphite oxidation reactions, especially at lower pressures. It was also observed that, besides H_2O, the OH species affects the nozzle recession rate greatly. For the metallized propellant, the concentrations of major oxidizing species such as H_2O, OH, and CO_2 are substantially reduced in comparison with the nonmetallized propellant, resulting in significant reduction of the erosion rates. A comparison of experimental data and predicted results from the graphite nozzle erosion minimization code shows excellent agreement especially for the nonmetallized propellant. To substantially reduce the throat recession rates at high pressures, it is suggested that the boundary-layer control at the throat region could be an effective method for future nozzle design considerations.

Nomenclature

A	=	cross-sectional area at the nozzle throat
A_s	=	preexponential factor in the Arrhenius reaction-rate expression
$A_{s,j}$	=	preexponential factor in the Arrhenius reaction-rate expression for jth reaction
C_c	=	thermal capacity of graphite
C_1	=	constant in k–ε model
C_2	=	constant in k–ε model
C_3	=	constant in k–ε model
C_4	=	constant in k–ε model
C_μ	=	constant in k–ε model
$E_{a,s}$	=	activation energy in the Arrhenius reaction-rate expression
$E_{a,s,j}$	=	activation energy in the Arrhenius reaction-rate expression for jth reaction
D	=	binary mass diffusivity of gas-phase species
Da	=	Damköhler number
D_i	=	binary mass diffusivity of ith gas-phase species
F	=	ratio of the overall erosion rate to diffusion-limited erosion rate
H	=	total enthalpy of the mixture $\sum_{i=1}^{N} Y_i h_i + \frac{1}{2}(u^2 + v^2)$
h_i	=	sensible enthalpy of ith gas-phase species
k	=	turbulent kinetic energy
Ma	=	Mach number
Ma_{c_L}	=	Mach number at the centerline of nozzle
Mw	=	molecular weight
Mw_c	=	molecular weight of carbon
Mw_i	=	molecular weight of ith gas-phase species
m	=	number
$\dot{m}''$	=	total mass rate of reaction with graphite per unit surface area
$\dot{m}_i''$	=	mass rate of chemical reaction of ith gas-phase species with graphite per unit surface area
N	=	number of gas-phase oxidizing species at the solid–gas interface
P	=	pressure
Pr	=	Prandtl number
Pr_t	=	turbulent Prandtl number
Prod_j	=	jth component of product species
P_i	=	partial pressure of ith gas-phase species (H_2O or CO_2)
q''	=	heat flux
$q''_{\mathrm{rad,net}}$	=	net radiation heat flux to the nozzle throat surface
r	=	radial coordinate
$\dot{r}_c$	=	net recession rate
$\dot{r}_{c,\mathrm{ch}}$	=	kinetic-limited recession rate
$\dot{r}_{c,d}$	=	diffusion-limited recession rate
$\dot{r}_i$	=	recession rate due to chemical reaction of ith gas-phase species (H_2O or CO_2) with graphite
R_o	=	outer radius of graphite nozzle
R_u	=	universal gas constant
S	=	surface area
Sc	=	Schmidt number
Sc_t	=	turbulent Schmidt number
S_1	=	interfacial surface area at the graphite-gas interface
T	=	temperature
T_c	=	temperature of graphite
T_{c_L}	=	temperature at centerline
T_{c_0}	=	initial temperature of graphite
T_s	=	surface temperature at the nozzle throat
T_{t,c_L}	=	total temperature at centerline (=)
t	=	time
U_b	=	bulk gas velocity component in axial direction
U_{c_L}	=	centerline gas velocity component in axial direction
u	=	gas velocity component in axial direction
v	=	gas velocity component in radial direction
x	=	axial coordinate
Y	=	mass fraction

Presented as Paper 0363 at the 44th AIAA Aerospace Sciences Meeting and Exhibit, Reno, Nevada, 9–12 January 2006; received 18 March 2006; revision received 19 April 2007; accepted for publication 23 April 2007.

*Ph.D. Candidate, Department of Mechanical and Nuclear Engineering, 137 Research Building East. Member AIAA.

†Distinguished Professor, Department of Mechanical and Nuclear Engineering, 140 Research Building East. Fellow AIAA.

Y_i = mass fraction of the ith gas-phase species
Y_{i,c_L} = mass fraction of the ith gas-phase species at centerline
α = thermal diffusivity of propellant
β_j = temperature exponent in the Arrhenius reaction-rate expression for jth reaction
γ = ratio of specific heat
ε = turbulence dissipation rate
λ = thermal conductivity
λ_c = thermal conductivity of graphite
λ_g = thermal conductivity of gas mixture
λ_s = thermal conductivity of solid conducting material at the outer surface of graphite nozzle
μ = viscosity
μ_{eff} = effective viscosity ($\mu_t + \mu$)
μ_t = turbulent viscosity
$\nu_{B,i}$ = stoichiometric coefficient of gas-phase oxidizing species in ith chemical reaction
$\nu_{C,i}$ = stoichiometric coefficient of graphite in ith chemical reaction
$\nu_{P,i}$ = stoichiometric coefficient of gas-phase product species in ith chemical reaction
ρ = density
ρ_b = bulk density of gas mixture
ρ_c = density of graphite
ρ_{c_L} = density of gas mixture at the centerline
ρ_g = density of gas-phase species
ρ_i = density of ith gas-phase species
ρ_i' = surface density of ith adsorbed gas-phase species
τ_w = shear stress at the wall
$\dot{\omega}_i$ = volumetric rate of reaction of ith chemical reaction

Subscripts:

b = bulk property
c = graphite
ch = chemical
c_L = centerline
d = diffusion
eff = effective value
g = gas phase
i = ith species index
j = jth species index
rad = radiation
s = surface
t = turbulent
0 = initial values

Superscript

$''$ = fluctuation quantity in Favre averaging

Diacriticals

$\tilde{}$ = mass weighted average quantity (Favre averaged)
$\bar{}$ = time averaged quantity (mean value)

I. Introduction

DURING rocket motor operating conditions, the surface of the graphite nozzle is subjected to very high heat fluxes. This causes an increase in the reactivity of the graphite material. Thus, the heterogeneous reaction rates with the oxidizing species (such as H_2O, OH, CO_2, O, and O_2) are increased even though the concentrations of O_2 and O are usually very low in the combustion products of solid rocket motors. The recession rate of the graphite nozzle throat by thermochemical erosion is also dependent on the diffusion rate of these oxidizing species near the surface region, as proposed in an analytical study by Delaney et al. [1] and McDonald and Hedman [2]. In addition to thermochemical erosion, the graphite material can also be consumed by a mechanical erosion mechanism. However, for high-density graphite with excellent mechanical properties, the mechanical erosion could be considered to be secondary to thermochemical erosion. The physical and chemical processes of graphite nozzle erosion are extremely complicated, as shown in Fig. 1.

To increase the range and performance of a rocket propulsion system, the operating pressures of future rocket motors will be much higher than the existing ones. The rocket motor pressures could reach the level of 4000–5000 psia in the near term and 8000–10,000 psia in the longer term. The increase of chamber pressure will result in a substantial increase of the heat-transfer rate from the high-temperature products to the nozzle material, especially at the nozzle throat. Furthermore, the flame temperatures of many advanced propellants are above 3600 K, which enhances thermal loading and chemical reactions at nozzle surfaces. Any throat erosion can cause severe performance reduction. Therefore, it is vitally important to study the fundamental interactions between the propellant combustion products and nozzle materials under these severe operating conditions.

In this study, we have selected two baseline propellants for studying the graphite nozzle erosion process. One propellant is a nonmetallized propellant (called propellant S) and the other is a metallized propellant (called propellant M). Propellant S is an ammonium perchlorate/hydroxyl-terminated polybutadiene (AP/HTPB) composite propellant with 87% solids loading, ~9% HTPB, and ~4% minor ingredients. Propellant M is also an AP/HTPB composite propellant with 19% aluminum. The selection of these two propellants is based upon several considerations, including 1) the normal composite propellant formulation used in military and industrial rocket propulsion applications; 2) their adequate combustion behavior at high pressures with reasonably low-pressure exponents; and 3) processing capability at our collaborating government laboratory at NAWC-China Lake.

The primary objective of this study is to advance a comprehensive model to predict the thermochemical erosion rate of a graphite nozzle and to study the effect of pressure and propellant formulation on the erosion rate behavior of graphite at ultrahigh pressures. This model considers both finite-rate heterogeneous kinetic schemes for graphite oxidation and the diffusion of oxidizing species to the nozzle throat surface. In this work, major oxidizing species have been identified and an extensive literature survey has been conducted to verify that

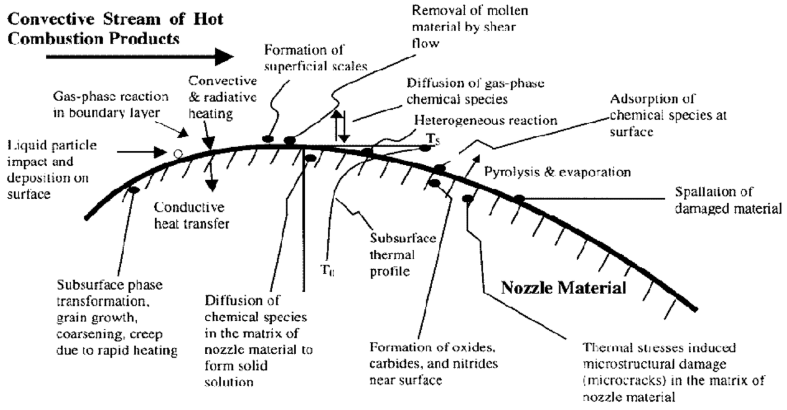

Fig. 1 Physical and chemical processes associated with the rocket nozzle erosion.

the Cl_2 and HCl have negligible effect on the graphite oxidation process. This work also provides a conclusive analysis for the relative importance of mass transfer and reaction kinetics in the nozzle throat erosion process. This paper addresses the likelihood of phase transformation of graphite into a highly reactive form called carbyne and the implications of this phenomenon on graphite throat recession.

II. Theoretical Formulation

A. Description of the Graphite Nozzle Erosion Minimization Code

The theoretical formulation for nozzle recession rate predictions was developed earlier by Kuo and coworkers [3–5]. The current graphite nozzle erosion minimization (GNEM) code is an upgraded numerical code that is based largely on the theoretical model developed in their work. The earlier version of this model and numerical code was validated by using experimental data obtained from several different rocket motor firings, including the BATES (ballistic test and evaluation system) motor by Geisler [6], the MERM (material evaluation rocket motor) motor by Klager [7], and the HIPPO (high-pressure motor) by Dirling et al.[‡].

The GNEM code solves the combined core flow and viscous shear flow regions through a 2-D or axisymmetric nozzle. The flow in the core region is considered one dimensional, compressible, invisicid, and quasi steady. The flow near the nozzle surface is considered planar or axisymmetric, viscous, and quasi steady due to the relatively slow surface regression rate. The heat conduction process in the nozzle material is considered planar or axisymmetric and unsteady. The nozzle material properties are evaluated as functions of local temperature. The instantaneous governing equations have been Favre averaged to arrive at mean governing equations. A second-order k–ε turbulence model has been used to achieve closure of the turbulent flow problem. This code can solve flat plate or cylindrical boundary-layer problems with close prediction of measured data of turbulence variables, velocity, and temperature profiles. The code is based on the GENMIX numerical procedure proposed by Patankar and Spalding [8]. This code has been revitalized to facilitate the nozzle erosion study at high-pressure conditions. The boundary layer is considered to be quasi steady, planar or axisymmetric, and chemically reacting.

As the propellant in the rocket motor burns, the nozzle is exposed to hot combustion products, which form a turbulent boundary layer over the nozzle surface. The hot products transfer energy to the nozzle, causing its surface temperature to rise rapidly. The high surface temperatures of the nozzle increase the reactivity of the graphite and heterogeneous reaction rates with gaseous oxidizing species, which are produced as a result of propellant combustion. These surface reactions result in recession of the graphite nozzle surface. Since the heat-transfer coefficient is much higher at the nozzle throat than any other axial position in the nozzle, the surface reaction is dominant at the throat. Because of the surface reactions, the concentration of oxidizing species available at the nozzle surface decreases, which creates concentration gradients in the flowfield. This causes mass diffusion of oxidizing species toward the nozzle surface. In order for the surface reactions to continue, the oxidizing species must diffuse to the nozzle surface to react with graphite. Therefore, the rate of nozzle recession depends on the diffusion rate of oxidizing species to the surface. However, because these surface reactions also have a finite time associated with them, the kinetic rates of these reactions also affect the recession rate of the graphite surface at the nozzle throat. Thus, both the chemical kinetic rates of the heterogeneous reactions and the diffusion rate of oxidizing species to the surface determine the nozzle recession rate at the throat.

When the kinetic rates are much higher than the diffusion rates (high Damköhler number situation), the recession rate is determined mainly by the diffusion rate of the oxidizing species. This recession rate is identified as $\dot{r}_{c,d}$. In this case, the diffusion-limited erosion rate of graphite is given as follows [3]:

$$\dot{r}_c = \dot{r}_{c,d} = \frac{Mw_c}{\rho_c} \sum_{i=1}^{N} \frac{(\rho_i D_i)_{\text{eff}}}{Mw_i} \left. \frac{\partial Y_i}{\partial r} \right|_s \tag{1}$$

In the above equation, ρ_c is the density of graphite, Mw_c is the molecular weight of graphite, Y_i is the mass fraction of the ith oxidizing gaseous species, ρ_i is the density of the ith gaseous species at the gas–solid interface, D_i is the binary gas diffusivity of the ith species with the mixture, and N is the total number of gaseous oxidizing species.

The other extreme case is the case of high diffusion rates and low kinetics rates (low Damköhler number situation), with the recession rate solely determined by the chemical kinetics. This recession rate is identified as $\dot{r}_{c,\text{ch}}$. In this case, the erosion rate of graphite is given as follows:

$$\dot{r}_c = \dot{r}_{c,\text{ch}} = \frac{1}{\rho_c} \sum_{i=1}^{N} \dot{m}_i'' \tag{2}$$

where $\dot{m}_i''$ is the mass rate of reaction of the ith species with graphite per unit area. If the diffusion rates and kinetic rates are of the same order, then the overall recession rate $\dot{r}_c$ can be calculated from the following equation:

$$\frac{1}{\dot{r}_c} = \frac{1}{\dot{r}_{c,d}} + \frac{1}{\dot{r}_{c,\text{ch}}} \tag{3}$$

The above equation is equivalent to the equation for calculating total resistance of an electric circuit with two resistances connected in series. The inverse of the overall erosion rate is then equal to the sum of the inverse of the diffusion-limited erosion rate and the inverse of the kinetic-limited erosion rate.

It can be seen from Eq. (3) that if either $\dot{r}_{c,d}$ or $\dot{r}_{c,\text{ch}}$ is much larger than the other, the smaller one will be the rate controlling factor. Thus, a dimensionless factor F can be defined as the ratio of the overall erosion rate to the diffusion-limited erosion rate such that, as $F \to 1$, the erosion process is diffusion controlled and, as $F \to 0$, the erosion process is kinetic controlled.

$$F \equiv \frac{\dot{r}_c}{\dot{r}_{c,d}} \quad \text{and} \quad 1 - F = \frac{\dot{r}_c}{\dot{r}_{c,\text{ch}}} \tag{4}$$

The diffusion-limited erosion rate $\dot{r}_{c,d}$ depends on the concentration gradients of oxidizing species at the nozzle surface, the density of the gas at the nozzle surface, and the concentration of oxidizing species in the core region. These parameters in turn depend on the chamber pressure, temperature, consumption of gaseous species in heterogeneous reactions at the graphite surface, and turbulence level in the shear flow. The gas-phase conservation equations are solved for the flow property distributions to determine $\dot{r}_{c,d}$. The kinetic-limited erosion rate $\dot{r}_{c,\text{ch}}$ depends on the kinetic constants of the heterogeneous reactions, the concentration of the oxidizing species, and the surface temperature of the nozzle. Thus, the surface temperature is determined by solving the transient heat conduction equation for the graphite nozzle to compute $\dot{r}_{c,\text{ch}}$. Once $\dot{r}_{c,d}$ and $\dot{r}_{c,\text{ch}}$ have been determined, the recession rate $\dot{r}_c$ can be obtained from Eq. (3). The parameter F can be related to the Damköhler number by the following relationship as given by Eq. (5):

$$F \propto \frac{Da}{1 + Da} \tag{5}$$

The reason for not directly using the Damköhler number in our analysis is the fact that the Damköhler number by definition is the ratio of species diffusion time and chemical reaction time. In this study, there is no direct way to evaluate these characteristic times. On the other hand, the factor F is a more convenient parameter for comparing the relative importance of nozzle erosion rate dominated by chemical kinetics versus the nozzle erosion rate dominated by the diffusion of oxidizing species to the nozzle surface.

[‡]Dirling, R. B., Jr., Heightland, C. N., Loomis, W. C., Ellis, R. A., and Kearney, A. J. (private communication), 1983.

B. Governing Equations of the GNEM Model

The formulation of the theoretical model involves the general conservation equations for the gas phase and the solid phase. The gas-phase conservation equations consist of equations for the viscous boundary-layer flow region and the inviscid core region. The solid-phase conservation equation is the transient heat conduction equation for the nozzle material.

1. *Conservation Equations for the Boundary-Layer Flow Region*

Major assumptions made in this analysis are as follows: 1) averaged flow properties are quasi steady due to a relatively steady operation of the rocket motor, 2) body forces are negligible, 3) radiative energy transfer is small in comparison with convective energy transfer, 4) Soret or Dufour effects are very small, 5) turbulent Lewis number is equal to unity, 6) Fick's law of diffusion is valid, and 7) gas-phase reactions have negligible effects on the recession process and the concentrations of gas-phase species in the core region are determined by the equilibrium composition of the propellant combustion products. The last assumption is justified due to extremely low concentration of O_2 in the products, which prevents the oxidation reaction of H_2 and CO into H_2O and CO_2, respectively. Therefore, the gas-phase reactions can hardly alter the concentration profiles of reactants like H_2O and CO_2. The rates of heterogeneous reactions at the surface are significantly smaller than the rates of supply of the gas-phase species from the combustion chamber to the core region at the nozzle throat. Thus, the heterogeneous reactions would not alter the concentration of gaseous species in the core region by any significant amount.

A second-order two-equation k–ε turbulence model has been used to achieve closure of the turbulent flow problem. Using the aforementioned assumptions and following an order-of-magnitude analysis, conservation equations for mass, momentum, species, enthalpy, turbulent kinetic energy, turbulent dissipation, and equation of state are as follows:

$$\frac{\partial}{\partial x}(r^m \bar{\rho}\,\tilde{u}) + \frac{\partial}{\partial r}(r^m \bar{\rho}\,\tilde{v}) = 0 \tag{6}$$

$$\bar{\rho}\,\tilde{u}\frac{\partial \tilde{u}}{\partial x} + \bar{\rho}\,\tilde{v}\frac{\partial \tilde{v}}{\partial r} = \frac{1}{r^m}\frac{\partial}{\partial r}\left[r^m \mu_{\text{eff}}\frac{\partial \tilde{u}}{\partial r}\right] - \frac{\mathrm{d}\bar{p}}{\mathrm{d}x} \tag{7}$$

$$\bar{\rho}\,\tilde{u}\frac{\partial \tilde{Y}_i}{\partial x} + \bar{\rho}\,\tilde{v}\frac{\partial \tilde{Y}_i}{\partial r} = \frac{1}{r^m}\frac{\partial}{\partial r}\left[r^m \left(\frac{\mu}{Sc}\right)_{\text{eff}}\frac{\partial \tilde{Y}_i}{\partial r}\right] + \bar{\dot{\omega}}_i \tag{8}$$

$$\bar{\rho}\,\tilde{u}\frac{\partial \tilde{H}}{\partial x} + \bar{\rho}\,\tilde{v}\frac{\partial \tilde{H}}{\partial r} = \frac{1}{r^m}\frac{\partial}{\partial r}\left[r^m \left(\frac{\mu}{Pr}\right)_{\text{eff}}\frac{\partial \tilde{H}}{\partial r} + \left\{\mu_{\text{eff}} - \left(\frac{\mu}{Pr}\right)_{\text{eff}}\right\}\frac{\partial \tilde{u}^2/2}{\partial r}\right] \tag{9}$$

$$\bar{\rho}\,\tilde{u}\frac{\partial k}{\partial x} + \bar{\rho}\,\tilde{v}\frac{\partial k}{\partial r} = \frac{1}{r^m}\frac{\partial}{\partial r}\left[r^m\left(\mu + \frac{\mu_t}{C_1}\right)\frac{\partial k}{\partial r}\right] + \mu_t\left[\frac{\partial \tilde{u}}{\partial r}\right]^2 - \bar{\rho}\varepsilon \tag{10}$$

$$\bar{\rho}\,\tilde{u}\frac{\partial \varepsilon}{\partial x} + \bar{\rho}\,\tilde{v}\frac{\partial \varepsilon}{\partial r} = \frac{1}{r^m}\frac{\partial}{\partial r}\left[r^m\left(\mu + \frac{\mu_t}{C_2}\right)\frac{\partial \varepsilon}{\partial r}\right] + C_3\mu_t\left[\frac{\partial \tilde{u}}{\partial r}\right]^2\frac{\varepsilon}{k} - C_4\bar{\rho}\frac{\varepsilon^2}{k} \tag{11}$$

$$\bar{p} = \bar{\rho}R_u\tilde{T}/\overline{Mw} \tag{12}$$

where $m = 0$ for planar flows and $m = 1$ for axisymmetric flows. The turbulent viscosity μ_t is expressed in terms of k and ε based upon the following Prandtl–Kolmogorov relationship:

$$\mu_t = C_\mu\bar{\rho}\frac{k^2}{\varepsilon} \propto \bar{p} \tag{13}$$

Because k and ε are both kinematic parameters, the group k^2/ε is also a kinematic parameter, which is independent of pressure. Therefore, the only pressure dependency component is density. For any fluid in turbulent flow, we have

$$(\rho D)_{\text{eff}} = \left(\frac{\mu}{Sc}\right)_{\text{eff}} = \left(\frac{\mu}{Sc}\right)_{\text{laminar}} + \left(\frac{\mu}{Sc}\right)_{\text{turbulent}} = \frac{\mu}{Sc} + \frac{\mu_t}{Sc_t} \approx \frac{\mu_t}{Sc_t} \tag{14}$$

The following Boussinesq approximations have been used to obtain Eqs. (6–11):

$$-\overline{\rho u'' v''} = \mu_t\frac{\partial \tilde{u}}{\partial r} \tag{15}$$

$$-\overline{\rho v'' Y_i''} = \frac{\mu_t}{Sc_t}\frac{\partial \tilde{Y}_i}{\partial r} \tag{16}$$

$$-\overline{\rho v'' h_i''} = \frac{\mu_t}{Pr_t}\frac{\partial \tilde{h}_i}{\partial r} \tag{17}$$

Values of the turbulence constants used in this modeling are listed in Table 1. These constants have been successfully tested before.

2. *Governing Equations for the Inviscid Region*

In the potential flow region of the developing flow, the following set of equations has been used:

$$\rho_{c_L}U_{c_L}\frac{\mathrm{d}U_{c_L}}{\mathrm{d}x} = -\frac{\mathrm{d}\bar{p}}{\mathrm{d}x} \tag{18}$$

$$T_{c_L} = \frac{T_{tc_L}}{\{1 + [(\gamma - 1)/2]Ma_{c_L}^2\}} \tag{19}$$

The centerline velocity U_{c_L} is calculated from Eq. (18) and the axial pressure gradient is calculated from the overall momentum balance by using the following equations written in terms of bulk flow properties ρ_b and U_b as follows:

Table 1 Constants used in turbulence modeling

Constant	C_1	C_2	C_3	C_4	C_μ
Value	1.0	1.3	1.57	2.0	0.09
Reference	Launder & Spalding [9] (1972) Lockwood & Naguib [11] (1975) Gosman [10] (1976)	Launder & Spalding [9] (1972) Lockwood & Naguib [11] (1975) Gosman [10] (1976)	Gosman [10] (1976) —— ——	Lockwood & Naguib [11] (1975) —— ——	Launder & Spalding [9] (1972) Lockwood & Naguib [11] (1975) Gosman [10] (1976)

$$\frac{\mathrm{d}\bar{p}}{\mathrm{d}x} = \left[2\pi R\tau_w + \frac{\mathrm{d}}{\mathrm{d}x}(\rho_b A U_b^2)\right] \Big/ A \tag{20}$$

$$\frac{\mathrm{d}}{\mathrm{d}x}(\rho_b U_b A) = 2\pi R \rho_c \dot{r}_c \tag{21}$$

The pressure gradient given by Eq. (20) includes the effect of change in the flow area and the change in bulk flow variables along the axial direction. Equation (21) is obtained from the overall mass balance inside the nozzle.

3. Transient Heat Conduction Equation in the Solid Phase

It is assumed that the heat conduction into the nozzle material is dominant in a direction normal to the nozzle surface. In a coordinate system attached to the recessing surface, the temperature distribution in the nozzle material at a given axial location along the surface is governed by the following equation:

$$\frac{\partial}{\partial t}(\rho_c C_c T_c) = \frac{1}{r^m}\frac{\partial}{\partial r}\left(\lambda_c r^m \frac{\partial T_c}{\partial r}\right) + \dot{r}_c \frac{\partial}{\partial r}(\rho_c C_c T_c) \tag{22}$$

The thermal properties of nozzle material such as ρ_c, C_c, and λ_c are allowed to vary with temperature.

4. Boundary and Initial Conditions

To complete the formulation of the theoretical model the boundary conditions are specified at the solid–gas interface as well as the freestream. At the solid–gas interface, the mass and energy balance lead to the following boundary conditions:

$$\underbrace{(\bar{\rho}\,\tilde{v}\,\tilde{Y}_i)_g}_{\substack{\text{mass flux of the}\\ i\text{th species}\\ \text{convected from}\\ \text{the surface}}} + \underbrace{\left(\bar{\rho}D\frac{\partial \tilde{Y}_i}{\partial r}\right)_g}_{\substack{\text{mass flux diffused}\\ \text{from the surface}}} = \underbrace{\dot{\omega}_i}_{\substack{\text{rate of generation}\\ \text{of the } i\text{th species}\\ \text{at the surface per}\\ \text{unit area}}} - \underbrace{\frac{1}{A}\frac{\mathrm{d}}{\mathrm{d}t}\iint_{S_1}\rho_i' \,\mathrm{d}S}_{\substack{\text{rate of mass}\\ \text{accumulation}\\ \text{of the } i\text{th species}\\ \text{per unit area}}} + \underbrace{(\rho_c \dot{r}_c \tilde{Y}_i)}_{\substack{\text{mass flux of}\\ \text{the } i\text{th species}\\ \text{fed to the surface}\\ \text{due to the surface}\\ \text{regression}}} \tag{23}$$

$$\lambda_g \left.\frac{\partial \tilde{T}}{\partial r}\right|_g + q''_{\text{rad,net}} + \sum_{i=1}^{N} \tilde{h}_i \left(\dot{\omega}_i - \frac{1}{A}\frac{\mathrm{d}}{\mathrm{d}t}\iint_{S_1}\rho_i' \,\mathrm{d}S\right) = \lambda_c \left.\frac{\partial T_c}{\partial r}\right|_c \tag{24}$$

In this formulation, the r direction is defined as the direction of the radial vector from the centerline of the nozzle. In Eqs. (23) and (24) ρ_i' is defined as the surface density of adsorbed gaseous species and S_1 is the interfacial surface area. The other boundary conditions at the solid–gas interface are as follows:

$$\tilde{u} = 0, \qquad \tilde{T} = T_s, \qquad \tilde{v} = -\rho_c \dot{r}_c / \rho_g \tag{25}$$

At the edge of the boundary layer:

$$\tilde{u} = U_{c_L}, \qquad \tilde{T} = T_{c_L}, \qquad \tilde{Y}_i = Y_{i,c_L}, \quad \text{and} \quad \frac{\partial \kappa}{\partial r} = \frac{\partial \varepsilon}{\partial r} = 0 \tag{26}$$

where U_c and T_c are obtained from potential flow analysis.

For the solid phase, the other boundary condition is provided either by the adiabatic condition at the outer radius if the nozzle is covered effectively by an insulation material or by heat flux balance at the outer radius if the graphite nozzle is in contact with a conductive material. For these two conditions, we have

$$\left.\frac{\partial T_c}{\partial r}\right|_{r=R_o} = 0 \quad \text{or} \quad \lambda_c \left.\frac{\partial T_c}{\partial r}\right|_{r=R_o} = \lambda_s \left.\frac{\partial T_s}{\partial r}\right|_{r=R_o} \tag{27}$$

The initial condition for the solid-phase heat conduction is as follows: $T_c = T_{c_0}$ at $t = 0$.

For the case of the diffusion-controlled recession process, the concentration of reactant at the gas–solid interface is very small, that is,

$$(\tilde{Y}_i)_g \approx 0 \tag{28}$$

This permits the solution of the species equations and the calculation of $\dot{\omega}_i$ using Eq. (23). If the reaction between a reactant B_i and graphite can be represented as

$$\nu_{c,i} C_s + \nu_{B,i} B_i \rightarrow \sum_j \nu_j \mathrm{Pr\,od}_j \tag{29}$$

then the recession rate of the graphite surface can be expressed as

$$\dot{r}_{c,d} = \frac{1}{\rho_c}\sum_i \dot{\omega}_i \frac{\nu_{c,i} M w_c}{\nu_{B,i} M w_{B_i}} \tag{30}$$

5. Heterogeneous Reaction Kinetics

a. Heterogeneous reaction-rate considerations. Extensive literature review was conducted to investigate the reactions of graphite with various gaseous species found in the combustion products of propellant S (i.e., H_2O, HCl, CO_2, N_2, CO, H_2, OH, H, O_2, and O). In these products, only H_2O, CO_2, CO, and OH are found in a significant amount for oxidizing reaction considerations. For propellant M, due to the formation of a significant amount of Al_2O_3 in the product of this metallized propellant, the mole fractions of H_2O and CO_2 are substantially lower than those of propellant S. In both propellants, the water vapor is the most important oxidizing species for graphite. The second important oxidizing species is OH radical and its concentration does not change much between propellant M and propellant S. Libby and Blake [12,13] provided the following Arrhenius expression for the reaction rate of H_2O and CO_2 with $C_{(s)}$ while considering the specific rates of both reactions to be equal:

$$\dot{r}_j = \frac{A_s P_j}{\rho_c}\exp\left(-\frac{E_{a,s}}{R_u T_s}\right) \tag{31}$$

$$\dot{r}_{c,\mathrm{ch}} = \sum_{j=1}^{N} \dot{r}_j = \sum_{j=1}^{N} \frac{A_s P_j}{\rho_c}\exp\left(-\frac{E_{a,s}}{R_u T_s}\right) \tag{32}$$

$j = 1$ for H_2O, $\quad j = 2$ for CO_2

The activation energy and the preexponential factor in the above case are 41.9 Kcal/mol and 2470 kg/(m^2 · s · atm), respectively. However, the kinetic data obtained by Golovina [14] gives the activation energy and the preexponential factor in the above case as 40 Kcal/mol and 158 kg/(m^2 · s · atm), respectively. The unit for the rate of reaction $\dot{r}_j$ is m/s.

These two reaction mechanisms considered global heterogeneous reactions of graphite with only the major species, that is, H_2O and CO_2, and the reactions of graphite with the gas-phase radical species were not taken into account. Recently, Chelliah et al. [15,16] used semiglobal heterogeneous chemical kinetics with reactions of graphite with H_2O, CO_2, OH, O_2, and O for numerical simulation of oxidation of a graphite rod. The reaction kinetics parameters were determined by various groups [17–29] for oxidation of graphite by H_2O, CO_2, OH, O_2, and O and those are listed in Table 2. These kinetic parameters were determined for nonporous graphite. Because the time scale associated with the diffusion of oxidizing species in the pores of the nozzle material is much longer than the duration of motor

firing, all of the heterogeneous reactions are assumed to be confined to the nozzle surface. Earlier Bradley et al. [30] employed this semiglobal heterogeneous reaction mechanism for oxidation of graphite particles and identified a free radical attack as the principle means of graphite oxidation.

The combustion products of propellants S and M contain a very small mole fraction of O radical (∼0.004%) and O_2 in comparison with other species. Therefore, reactions 2 and 5–8 are least important in the overall heterogeneous reaction mechanism. Even though reaction 3 is relatively slower compared to reaction 1, there is a very high mole fraction (∼43%) of H_2O in the products of propellant S; therefore, the oxidation of graphite by water vapor is dominant. In this case, the kinetic-limited erosion rate of graphite $\dot{r}_{c,\mathrm{ch}}$ is given as follows:

$$\dot{r}_{c,\mathrm{ch}} = \frac{1}{\rho_c} \sum_{j=1}^{N} k_j \prod_k P_k^{\nu_k} \tag{33}$$

The reaction-rate constant is assumed to follow the generalized Arrhenius form as given by

$$k_j = A_{s,j} T^{\beta_j} \exp\left(-\frac{E_{a,s,j}}{R_u T_s}\right) \tag{34}$$

For OH and O radicals, the reaction-rate constants were obtained by assuming the collision efficiencies at the graphite surface of 0.28 and 0.50, respectively [30]. In this work, we have examined the reaction-rate parameters proposed by the multiple oxidizing species (MOS) scheme for graphite oxidation reaction with OH. We have also compared the graphite nozzle erosion results predicted by MOS and a modified MOS (MMOS) with only a slight change of the temperature exponent from the value given by Neoh et al. [19] and a reduction of the preexponential factor for reaction 1. As shown in a later section, the MMOS scheme gives more satisfactory graphite nozzle throat erosion rate results. The kinetic parameters used in the MMOS for reaction 1 are shown in the bottom of Table 2. The kinetic parameters for the rest of the reactions are maintained the same as MOS.

In a paper by Hurt and Haynes [31], power-law kinetics of graphite oxidation with O_2 was studied. However, the reaction kinetics data proposed were applied to very low-temperature (<1000 K) and low-pressure (∼0.01 bar) conditions. In the paper by Sendt and Haynes [32], the chemisorption of O_2 on the armchair surface of graphite was studied, and two different reaction pathways were proposed and the associated activation energies for formation and desorption of CO molecules were evaluated. However, these data were also obtained for relatively lower temperature in comparison with the graphite nozzle surface temperature (∼2500 K). Therefore, our current modeling computations have been limited to semiglobal heterogeneous reaction mechanisms, similar to those employed by Bradley et al. [30] for modeling oxidation of graphite particles.

b. Justification for removing chlorine from the kinetic scheme. A literature survey was conducted to find the possible reactions and the reaction kinetics of halogens (particularly chlorine) with graphite. In the work by Freedman [33], the basal plane of graphite was exposed to beams of atomic and molecular fluorine and chlorine in an ultrahigh vacuum environment. X-ray photoelectron spectroscopy (XPS) and low-energy electron diffraction techniques were used to elucidate the chemistry involved. The carbon 1*s* XPS spectra of the halogenated highly ordered pyrolytic graphite (HOPG) graphite basal plane, which have been exposed to atomic chlorine, were compared to those of annealed samples of graphite. It was found that both spectra were identical to each other. This implies that exposure of the HOPG substrates to molecular chlorine produced no evidence of any uptake of chlorine. Furthermore, only an extremely small quantity (barely above the noise level) of chlorine could be measured by monitoring the 2*p* peak of Cl. This small quantity of adsorbed chlorine could be the result of the presence of edge planes exposed during the cleaving process; the edge plane of graphite is much more reactive than the basal plane. These results were in accordance with high-pressure data, which indicate that graphite

Table 2 Heterogeneous reaction-rate constants for nonporous graphite

Reference	Temperature range, K	Reaction	Reaction-rate parameters k_j, kg · m^{-2} · s^{-1} · atm^{-1}				Reaction rate R_j, kg · m^{-2} · s^{-1}
			j	β_j	$A_{s,j}$	$E_{a,s,j}$, Kcal/mol	
Sarofim & coworkers [19]	1575–1685	$C_{(s)} + OH \rightarrow CO + H$	1	−0.5	361 kg · K$^{0.5}$ · m^{-2} · s^{-1} · atm^{-1}	0.0	$R_1 = k_1 P_{OH}$
Rosner & Allendorf [17]	1100–2100	$C_{(s)} + O \rightarrow CO$	2	−0.5	665.5 kg · K$^{0.5}$ · m^{-2} · s^{-1} · atm^{-1}	0.0	$R_2 = k_2 P_O$
Bonnetain & Hoynant [18]	800–2500	$C_{(s)} + H_2O \rightarrow CO + H_2$	3[a,b]	0.0	4.80×10^5 kg · m^{-2} · s^{-1} · atm$^{-0.5}$	68.8	$R_3 = k_3 P_{H_2O}^{0.5}$
Bonnetain & Hoynant [18]	800–2500	$C_{(s)} + CO_2 \rightarrow 2CO$	4[a,c]	0.0	9.00×10^3 kg · m^{-2} · s^{-1} · atm$^{-0.5}$	68.1	$R_4 = k_4 P_{CO_2}^{0.5}$
			5	0.0	2.40×10^3 kg · m^{-2} · s^{-1} · atm^{-1}	30.0	$R_5 = \frac{k_5 P_{O_2} Y}{1 + k_6 P_{O_2}} + k_7 P_{O_2} (1 - Y)$
Nagle & Strickland- Constable [20]	1273–2273	$C_{(s)} + 1/2O_2 \rightarrow CO$	6	0.0	21.3×10^3 atm^{-1}	−4.1	$Y = [1 + \frac{k_8}{k_7 P_{O_2}}]^{-1}$
			7	0.0	0.535 kg · m^{-2} · s^{-1} · atm^{-1}	15.2	
			8	0.0	1.81×10^7 kg · m^{-2} · s^{-1}	97.0	
Modified reaction 1 (with OH) in MMOS	1575–1685	$C_{(s)} + OH \rightarrow CO + H$	1	−0.62	100 kg · K$^{0.62}$ · m^{-2} · s^{-1} · atm^{-1}	0.0	$R_1 = k_1' P_{OH}$

[a]The Arrhenius form of reactions 3 and 4 are from least square regression, taken over all the intrinsic reactivities of various carbons. The data are corrected to 1 atm and an order of reaction of 0.5 was chosen.
[b]The data for reaction 3 were taken from [18,20–24]. The highest and lowest values differed only by a factor of 2 from the Arrhenius form.
[c]The data for reaction 4 were taken from [18,21,22,29–35]. The highest and lowest values differed only by a factor of 2 from the Arrhenius form.

etching by fluorine occurs primarily by attack at the edge (prism planes) of graphite.

The low reactivity of the graphite basal plane to chlorine (and fluorine) is ascribed to the combination of steric and energetic factors. This mitigates against the disruption of the infinite two-dimensional ring structure of the basal plane. The edge (prism) plane of graphite, on the other hand, contains dangling bonds, which are readily available for reaction. In another significant work by Gonzalez and coworkers [34], the oxidation reaction of carbon black, sucrose carbon, and graphite in the presence of chlorine was studied by thermal analysis [thermogravimeteric analysis (TGA) and differential thermal analysis (DTA)]. Heating in chlorine caused different degrees of mass increase in each of the three carbons, with two reaction zones due to physisorption and chemisorption of chlorine on the carbon surface. Heating the three carbons in a chlorine atmosphere showed that graphite exhibited the smallest mass gain (0.5%) of all three carbons. The chlorine uptake by graphite is due to the joint effect of physisorption at low temperatures (473–573 K) and chemisorption (above 673 K). It was also shown that the oxygen uptake by graphite does not change in the presence of chlorine and vice versa. Burning of the carbons in the presence of chlorine showed its inhibiting effect, being weakest in graphite. Oxidation in the absence of chlorine started at 933 K for graphite. When chlorine was present in the gaseous phase, oxidation started at 1043 K. However, because the temperatures at the nozzle surface are going to be much higher than 1043 K, this difference in the oxidation temperature is not important.

In another paper by Henning [35], it is shown and suggested that chlorine reacts with graphite at low temperatures only. The graphite sample used in their work was pitch-bonded graphite brominated in a carbon tetrachloride solution of bromine and it was suspended in liquid chlorine at −33°C. After three days the electrical resistance of the graphite sample decreases only by 0.1 Ω. In the vapor phase, the reaction was even slower. It was stated in a paper by Norman and coworkers [36] that the physisorbed chlorine on a carbon cloth had a large influence on the interaction of the carbon with water, while chemisorbed chlorine had only a small effect. Based on these studies, it can be concluded that the reaction of graphite with Cl is negligible and the presence of Cl atoms in the vicinity of the nozzle surface does not affect graphite reactions with other oxidizing species.

6. *Numerical Procedure*

The system of coupled, nonlinear partial differential equations was solved using a numerical technique proposed by Patankar and Spalding [8]. Several researchers have used this technique successfully. Patankar and Spalding introduced a transformation of coordinates in which the grid points always fit the boundary-layer region even while the thickness of the region is changing. The near-wall treatment of k and ε is based upon the modified Van Driest formula and the method suggested by Cebeci and Chang [37] as described by Kuo and Keswani in [3].

III. Discussion of Results

The GNEM calculations were performed with two objectives: 1) examine the effect of pressure on the graphite erosion rate, and 2) study the effect of propellant composition on the graphite erosion rate. In the investigation of these two effects, four different heterogeneous kinetic schemes proposed individually by Libby–Blake [12,13], Golovina [14], the MOS reaction mechanism [17–29], and the MMOS reaction mechanism were used. As shown in Figs. 2a and 2b, in general, the kinetic-limited recession rates for propellants S and M are greatest when the MOS reaction mechanism was used and lowest when the reaction kinetics by Golovina was used. The MMOS reaction mechanism shows different behavior at low- and high-pressure regimes. The MMOS reaction mechanism gives the lowest kinetic-limited erosion rate around 7 MPa (∼1000 psia) motor operating pressure, while at pressures above 28 MPa (∼4000 psia), it gives kinetic-limited rates higher than both Libby–Blake and Golovina reaction mechanisms. The nonlinear behavior of kinetic-limited erosion rates with pressure can be attributed to the non-Arrhenius nature of the OH reaction with graphite (reaction 1 in the MOS and MMOS reaction mechanisms). The kinetic-limited recession rates for propellant M are substantially higher than those of propellant S, because the adiabatic flame temperature of propellant M is about 500 K higher than that of propellant S, leading to higher nozzle surface temperatures.

For realistic conditions, the diffusion rate cannot be infinitely fast. Therefore, the net recession rate should be less than the kinetic-limited recession rate. As mentioned above, a factor F is defined to signify the relative dominance of diffusion and reaction kinetics in determining the net recession rate. When $F \to 1$, the erosion process becomes diffusion controlled (or diffusion limited); as $F \to 0$, the erosion process becomes kinetic controlled (or kinetic limited). It can be seen from Eq. (3) that if either $\dot{r}_{c,d}$ or $\dot{r}_{c,\mathrm{ch}}$ is much larger than the other, the smaller one will be the recession rate controlling one.

For a finite diffusion rate, the kinetic-limited recession rates using the MOS reactions mechanism are very high for both propellants, therefore the factor F is closer to 1 as shown in Figs. 3a and 3b. This means that the erosion process is controlled by a diffusion process and the diffusion-limited recession rate is very close to the net recession rate. On the other hand, when the MMOS kinetic scheme is used, factor F shows very different characteristics for propellants S

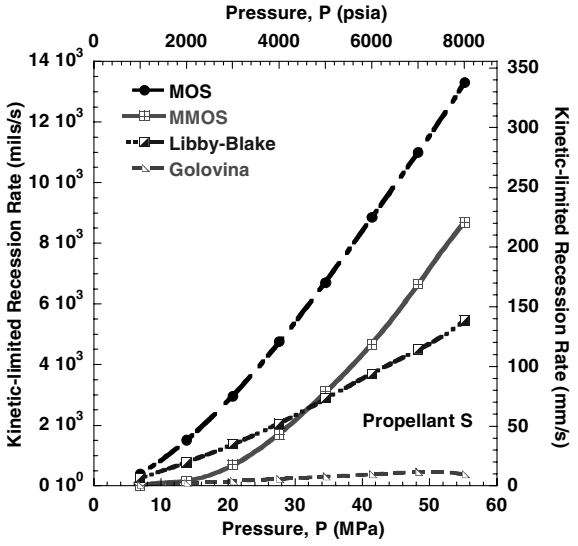

a) Propellant S

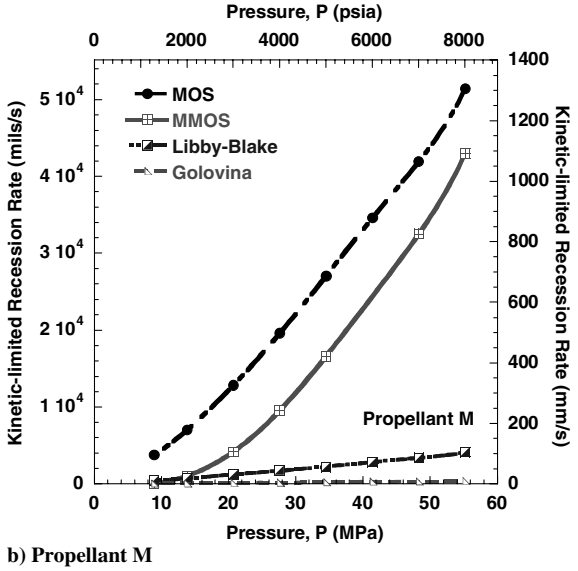

b) Propellant M

Fig. 2 Comparison of the kinetic-limited recession rate at the nozzle throat with Libby–Blake [12,13], Golovina [14], multiple oxidation species (MOS) mechanism [17–29], and MMOS reaction kinetics (assuming infinitely fast diffusion rate).

and M. In the low-pressure (∼15 MPa) regime, the factor F is smaller (<0.3) for propellant S indicating that the erosion process is controlled by heterogeneous surface reaction rates and thus the overall recession rate would be very close to the kinetic-limited recession rate. It should be noted that the MMOS reaction kinetic scheme shows very good agreement with the experimental erosion rate data. In the high-pressure regime, the factor F using MMOS is closer to 1 (>0.8), which implies that the erosion rate of the nozzle surface is a diffusion-controlled process. The Libby–Blake kinetic schemes imply that the erosion process is diffusion controlled at all pressures, while the Golovina kinetic scheme suggests the significant contribution of both rate of chemical reactions and rate of mass diffusion to the surface in the nozzle surface erosion process. In the case of propellant M, the factor F is close to 0.6 when Golovina kinetics is used indicating that both diffusion and kinetic rates are important. The MMOS reaction kinetic scheme suggests that at 7 MPa operating pressure, chemical kinetics plays an important role to determine the nozzle though erosion rates, whereas, at pressure higher than 7 MPa, the throat erosion rates are controlled by a diffusion process. The MOS and Libby–Blake kinetic schemes imply the throat erosion rates are diffusion controlled at all pressures. The above observations imply that a more accurate determination of surface kinetic schemes and reaction rates would lead to an accurate prediction of the recession rate at the nozzle throat. Thus, the controlling mechanism of the erosion process depends on both the reaction kinetics and the propellant composition.

The oxidizing species have to diffuse to the surface (by mass diffusion, advection processes by turbulent eddies, or combined diffusion-advection process) to react with the surface, and the net recession rate cannot be higher than the rate of diffusion of oxidizing species to the surface. This means that the diffusion-limited recession rate is the upper bound of the net recession rate. The lower bound of the net recession rate depends on a combination of reaction kinetics at the surface and a species diffusion rate to the surface.

It is shown in Figs. 4a and 4b that the net recession rate is higher when the rates of surface reactions are higher, which is the case when MOS reactions mechanism is used in comparison to Libby–Blake and Golovina. As shown in Figs. 2a and 2b, in the case of propellant S, kinetic-limited recession rates are different for the three reaction kinetic schemes. The rate of diffusion of species from the core region to the graphite surface depends on the rate of chemical reaction at the surface. Gas-phase species at the surface are consumed in the heterogeneous reactions between these species and the graphite surface. Because of this process, a concentration gradient is created between the core region and the surface, which governs the

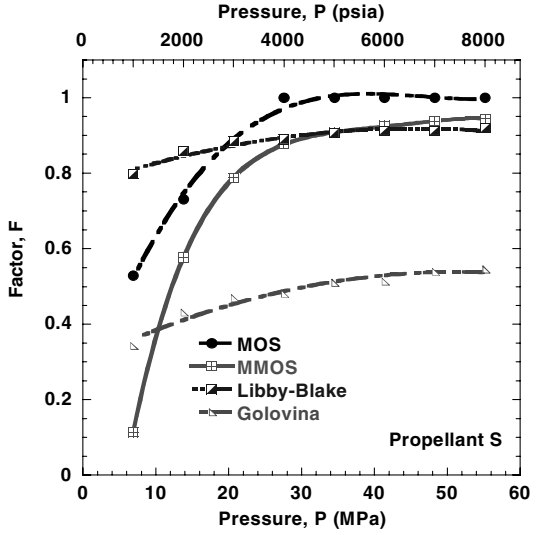

a) Propellant S

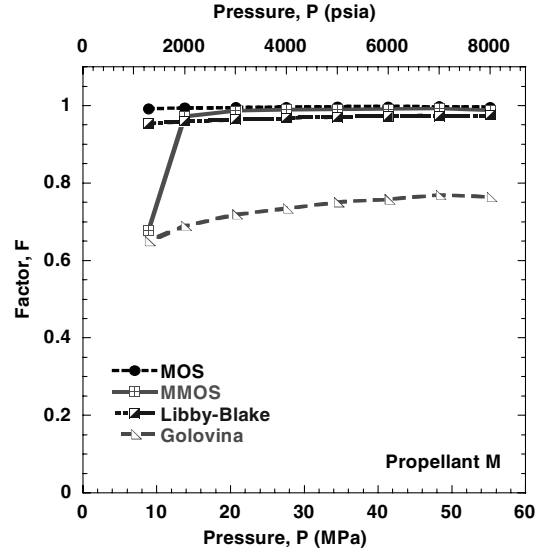

b) Propellant M

Fig. 3 Comparison of pressure dependence of the dimensionless factor F at the nozzle throat using Libby–Blake [12,13], Golovina [14], the MOS mechanism [17–29], and MMOS reaction kinetics.

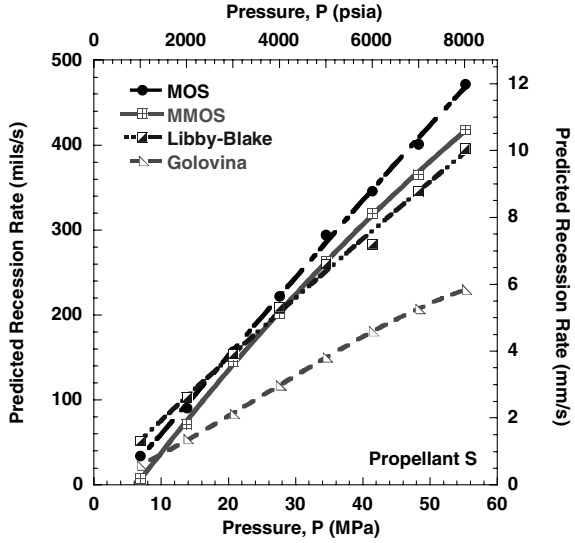

a) Propellant S

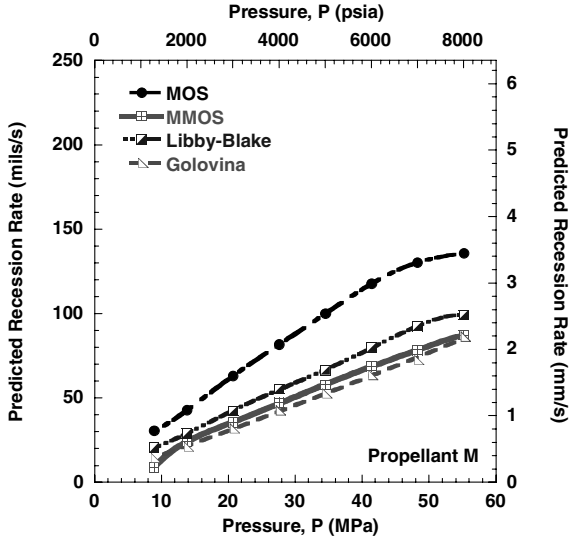

b) Propellant M

Fig. 4 Comparison of pressure dependence of the predicted graphite nozzle surface recession rates at the throat using Libby–Blake [12,13], Golovina [14], the MOS mechanism [17–29], and MMOS reaction kinetics.

species diffusion rate in the radial direction. If the heterogeneous reaction is faster, the gaseous oxidizing species would deplete faster and a higher concentration gradient is created resulting in a higher rate of mass diffusion to the surface. As both the rate of mass diffusion to the surface and the heterogeneous reaction rate are higher, the net recession rate of the graphite surface is higher. This explains the difference in the net recession rate prediction by the three reaction kinetic schemes. For both propellants S and M, the increase in pressure has a strong effect on the increase of the net recession rate. This is due to the fact that as pressure is increased, the density of product gases increases in the rocket motor. Based on the Prandtl–Kolmogorov relationship as shown in Eq. (12), the turbulent viscosity μ_t increases with gas density; therefore the effective turbulent diffusion rate also increases as shown in Eq. (13). Thus, the effective mass-diffusion rate of the ith oxidizing species, $(\rho D)_{\text{eff}} \partial Y_i / \partial r$, from the core region to the nozzle surface increases with pressure almost linearly. Because the mass flux at the nozzle surface increases with pressure, the net rate of reaction increases. Thus, the net recession rate increases with pressure almost linearly.

The magnitude of the predicted erosion rates for propellant S are substantially higher that those of propellant M. This is due to a large difference in the concentration of oxidizing species in the combustion products of these two propellants. Aluminum consumes most of the oxidizing species in the metallized propellant to form Al_2O_3 and other oxides of aluminum. Thus, less H_2O, OH, and CO_2 are available to react with graphite at the nozzle throat. The pressure dependency of mole fractions of major oxidizing species in the combustion products of both propellants is shown in Figs. 5a, 5b, 6a, and 6b. As shown in Fig. 5a, the mole fraction of H_2O does not vary with pressure for both propellants; however, the mole fraction of H_2O in the combustion products of propellant M is much less that of propellant S. Similarly, the mole fraction of CO_2 does not vary with pressure for both propellants. However, the mole fraction of CO_2 in the combustion products of propellant M is much less that of pPropellant S. Mole fractions of OH and O decrease drastically with pressure due to more effective three-body collisions at higher pressures but their concentration levels are similar for both propellants as shown in Figs. 6a and 6b, respectively.

The surface temperature comparisons for the three different kinetic schemes are shown in Figs. 7a and 7b for propellants S and M, respectively. The temperature at the nozzle throat surface is higher for the case when propellant M is used in the rocket motor because its adiabatic flame temperature is approximately 500 K higher than that of propellant S. The difference in surface temperature results while using different kinetic schemes is not very significant for both propellants indicating that the choice of kinetic scheme is not affecting surface temperature to a great extent. It is observed that predicted surface temperatures using multiple reaction mechanisms are slightly higher than the other two schemes. This could be caused by the exothermic reactions 2 and 5 in Table 2 and their higher rates

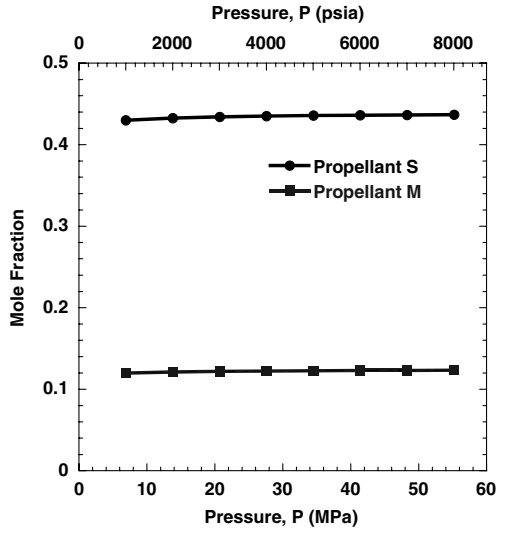

a) Mole fraction of H_2O

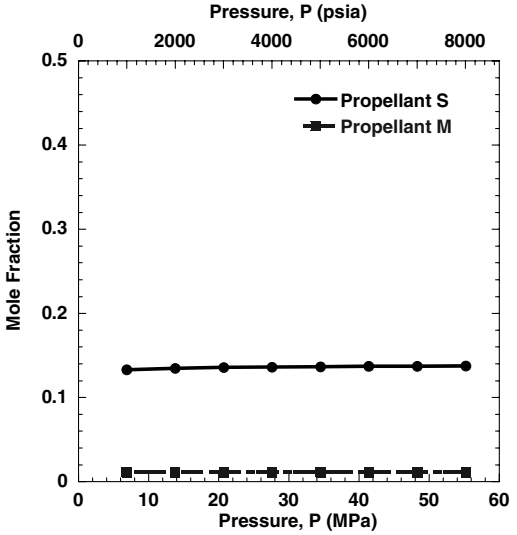

b) Mole fraction of CO_2

Fig. 5 Mole fractions of CO_2 and H_2O in combustion products of propellants S and M with pressure.

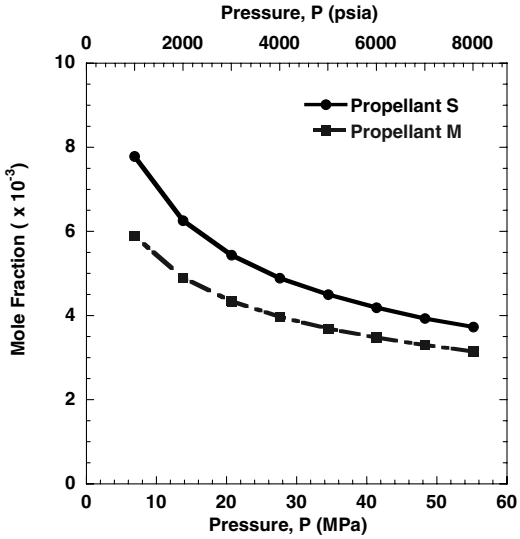

a) Mole fraction of OH

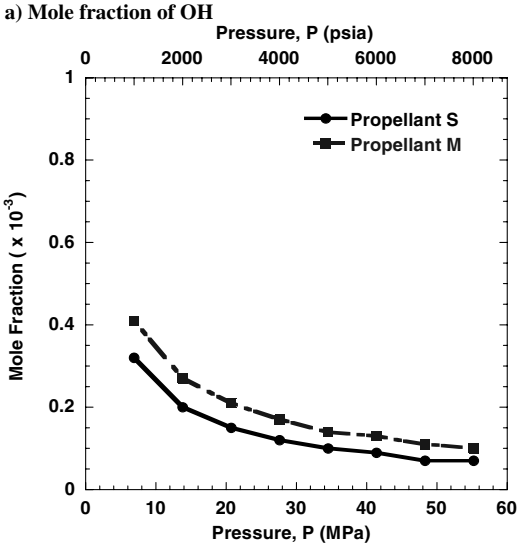

b) Mole fraction of O

Fig. 6 Pressure dependencies of mole fractions of OH and O in combustion products of propellants S and M.

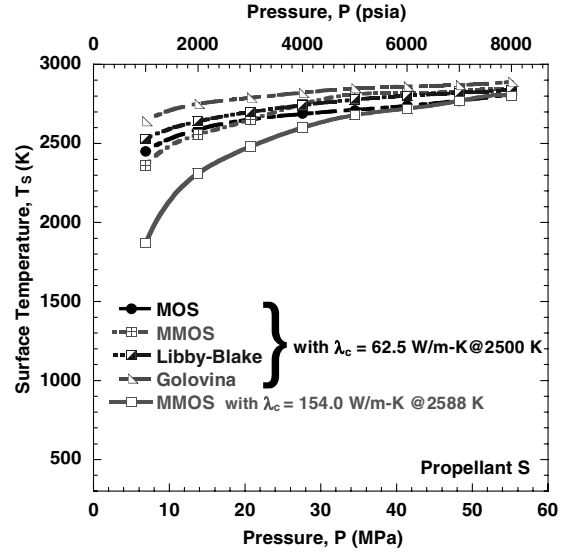

a) Propellant S

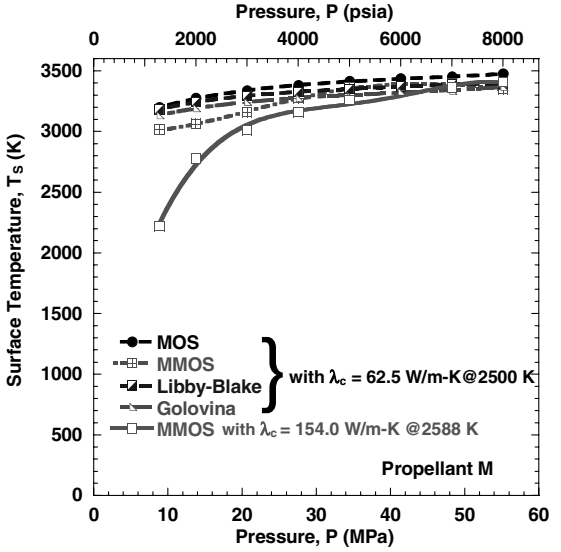

b) Propellant M

Fig. 7 Variation of surface temperature at the nozzle throat with operating pressure for both propellants using Libby–Blake [12,13], Golovina [14], the MOS mechanism [17–29], with $\lambda = 62.5$ W/m · K@2500 K and MMOS reaction kinetics with $\lambda = 154.0$ W/m · K@2588 K and $\lambda = 174.7$ W/m · K@300 K.

of reactions. These reactions are included in the multiple reactions kinetic scheme but not included in the other two kinetic schemes.

The variations of convective heat-transfer coefficients at the surface of the nozzle throat with pressure are shown in Figs. 8a and 8b for propellants S and M, respectively. The convective heat-transfer coefficient calculated using the Bartz correlation [38] at different pressures is also shown in these plots. In the original Bartz correlation, the pressure has an exponent of 0.8 with several other parameters (such as wall temperature, mixture viscosity, and mixture specific heat), which change with pressure due to the change in mixture composition with pressure. The Bartz correlation expressions shown in Fig. 8a for propellant S has a pressure exponent less than 0.8. This is caused by dependency of mixture composition on pressure. The heat-transfer coefficient for propellant S predicted by the GNEM code shows the same pressure exponents as given by the Bartz correlation. However, the coefficients from the GNEM predictions are about 25% higher than the results by the Bartz correlation. It is possible that the Bartz correlation was developed based upon experimental results of relatively cool propellant product gases than the propellants considered in this study.

The radiation heat-transfer coefficient is determined using the following equation:

$$\dot{q}''_{\text{radiation}} = \varepsilon\sigma\left(T_g^4 - T_s^4\right) \qquad h_{\text{rad}} = \dot{q}''_{\text{radiation}}/(T_g - T_s) \tag{35}$$

Blackbody radiation heat flux was calculated using emissivity of the gas-particle mixture as 1 and zero reflectivity from the graphite surface. It must be noted that emissivity of gas is much lower than 1 (∼0.01–0.04) and emissivity of soot (which is more emissive than Al particles) is in the range of 0.12–0.18 [39]. As shown in Figs. 8a and 8b, the equivalent blackbody radiation heat-transfer coefficient at the nozzle throat is an order of magnitude less than the convective heat-transfer coefficient. Therefore, radiation will not be a significant factor at the nozzle throat. Comparing the predicted nozzle erosion rates with the measured data from rocket motor firing using both propellants S and M tested the predictability of the GNEM code with the consideration of the MMOS kinetic scheme. The comparisons of the predicted and measured results are shown in Figs. 9 and 10 for propellants S and M, respectively. It is quite evident that these predictions are very close to the observed nozzle throat diameter variations, showing the capability of this upgraded GNEM code.

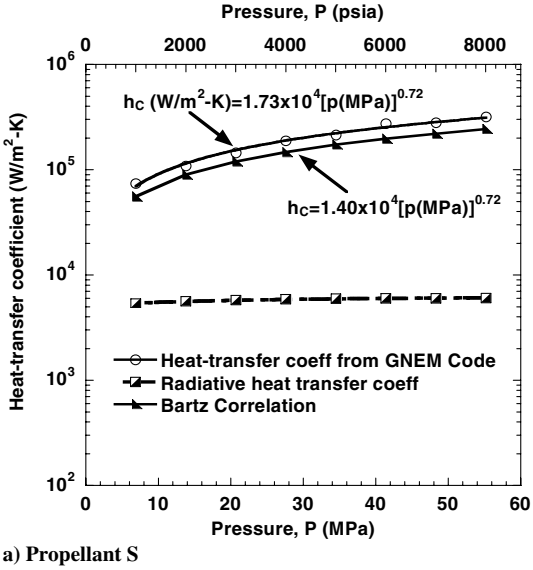

a) Propellant S

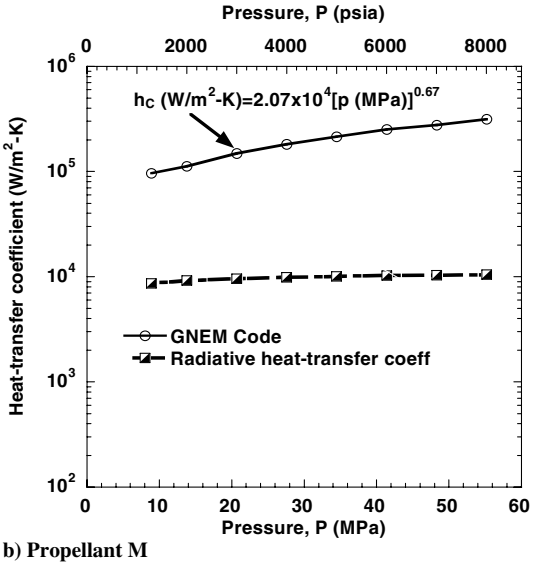

b) Propellant M

Fig. 8 Variation of heat-transfer coefficient at the nozzle throat with pressure and a comparison with calculated results from the Bartz correlation [34].

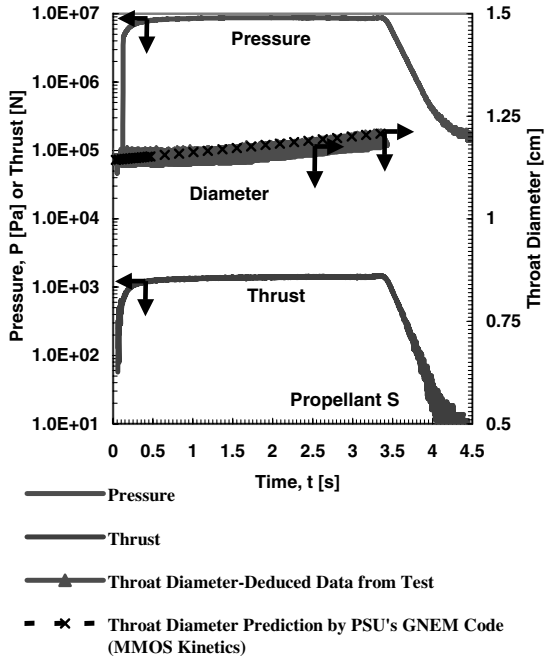

Fig. 9 Comparison of measured and predicted nozzle throat diameter variations in motor firing tests using propellant S.

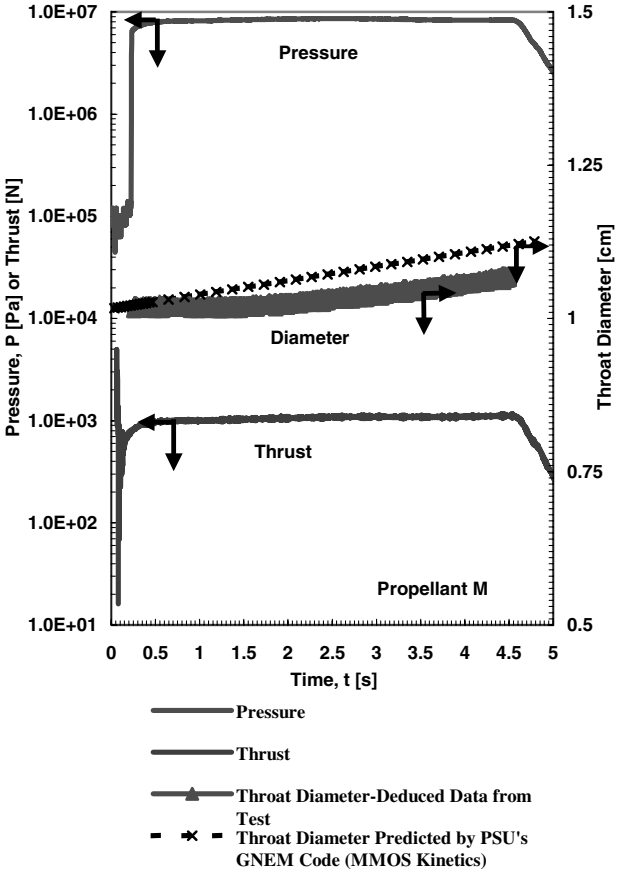

Fig. 10 Comparison of measured and predicted nozzle throat diameter variations in motor firing tests using propellant M.

IV. Conclusions

The thermochemical erosion rates of the graphite nozzle in rocket motors with two different propellants (a nonmetallized propellant S and a metallized propellant M) were predicted using a comprehensive reacting turbulent boundary-layer model with a k–ε turbulence closure for pressures from 7 to 55 MPa (1000 to 8000 psia). In these calculations, three different kinetic schemes and reaction-rate data proposed individually by Libby–Blake [12,13], Golovina [14], and MOS reactions mechanism [17–29] were considered for these two baseline propellants. It was found that the recession rate increases almost linearly with respect to pressure due to a higher rate of energy transfer, while the rate of increase depends on the choice of chemical kinetic scheme and propellant composition. For both propellants, the recession rates of the graphite nozzle are highest when the kinetic scheme and reaction-rate data of multiple reactions mechanism were used.

The major contribution of this paper is to assess the dependency of the erosion rate as a function of chamber pressure and propellant composition. At the present time, no ultrahigh pressure nozzle throat erosion data are available for further validation of the model. However, it is highly beneficial to study the effect of pressure on the erosion rate using the most updated graphite oxidation reaction kinetic schemes for the assessment of the erosion behavior. The MOS kinetic scheme is new to the erosion study. The findings about the strong pressure dependency up to pressures in the range of 21–55 MPa (3000–8000 psia) are very important because no similar work has been performed for such high-pressure levels.

The predicted results indicate that major oxidizing species are H_2O, OH, and CO_2. For a metallized propellant, the concentrations of these oxidizing species are substantially reduced in comparison with nonmetallized propellant due to the formation of aluminum oxides. This effect reduced the thermochemical attack by these oxidizing species on the graphite surface resulting in a significant reduction of the erosion rates. It is also shown that the overall throat recession rate of the graphite nozzle is a function of both the species diffusion rate and the heterogeneous reaction rate at the surface. In experimental work by Geisler et al. [6], a graphite nozzle erosion study was conducted with an aluminized propellant at an average chamber pressure of 1000 psia. In his work, BATES motors were used to provide recession data for the graphite nozzle. It was found that the presence of aluminum decreases the availability of oxidizers like H_2O, OH, and CO_2 in the gas mixture passing through the graphite nozzle and, therefore, it decreases the nozzle recession rate. This result is in agreement with the predicted nozzle recession rate comparisons between propellants S and M using the GNEM code.

The discovery of new carbon forms in 1968 by El Gorsey and Donnay [40], and Sladkov and Koudrayatsev [41] opened a field of research that revealed the behavior of carbon at high temperatures. The experimental work conducted many years ago by Kasatochkin et al. [42], and Nakamizo and Kammereck [43] indicated that the carbon forms contain –C ≡ C– units as chain. Whittaker [44] proposed that these forms occur due to a shift to triple bonding in the carbon system as temperature increases above 2600 K. Because acetylene is an organic molecule stable at high temperatures, it is reasonable to expect high-temperature carbon forms of this general structure. Based upon available research and analytical data on this phase-transformation process, at high temperatures, a single bond can break and shift an electron into each of the adjacent double bonds. This induces another single bond to break, such that one electron goes to the adjacent free radical double bond to form a triple bond and the other goes to the next adjacent double bond. If the process is repeated, the entire sheet of atoms separates into –C ≡ C– chains. When it does so, only electrons are shifted to rearrange bonds. This form of carbon is called carbyne. Because, in solid propellant rockets, the graphite nozzle surface temperature can reach 2600 K and higher, it is imperative to study this issue.

In experimental work by Geisler et al. [6], an abrupt increase in the nozzle throat erosion rate was observed at conditions corresponding to the attainment of a critical surface temperature around 2600 K. Therefore, he postulated that this phenomenon could be attributed to the graphite-to-carbyne phase transformation, which results in increased reactivity of the nozzle throat material. This postulation seems to be very reasonable and worthwhile for in-depth study. It is one of the topics of our current investigations and it is considered to be beyond the scope of this paper.

In view of the high rates of throat recession at high pressures, the boundary-layer control at the throat region seems to be a necessity in

order for rocket motor operation at these ultrahigh pressure conditions. The boundary-layer control mechanism should be designed to consume the oxidizing species near the surface of the nozzle throat so that the thermochemical attack can be substantially reduced, especially for nonmetallized propellant. In recent work by Acharya and Kuo [45], it was shown that the injection of this gas mixture not only reduces the temperature of combustion product gases in the boundary-layer region near the throat but also reduces the mass fraction of the oxidizing gaseous species such as H_2O, OH, and CO_2 in the combustion products. Thus, the erosion rates of the graphite nozzles at high-pressure operating conditions are significantly reduced by a factor up to 14, depending on the kinetic scheme adopted in the GNEM code. Experimentally, Wolt and Webber [46] have also shown this method to be very effective in reducing the erosion rates.

Acknowledgments

This research was conducted under the sponsorship of the Office of Naval Research (ONR) as a part of the multi-university research initiative (MURI) project funded under the Contract N00014-04-1-0683. The authors would like to acknowledge the interest, support, and encouragement of Judah Goldwasser of ONR. We would also like to acknowledge the invaluable suggestions made by Daniel O. Miller of NAWC-China Lake for the selection of baseline propellants and nozzle materials for this research study.

References

[1] Delaney, L. J., Eagleton, L. C., and Jones, W. H., "A Semi-Quantitative Prediction of the Erosion of Graphite Nozzle Inserts," *AIAA Journal*, Vol. 2, No. 8, Aug. 1964, pp. 1428–1433.

[2] McDonald, A. J., and Hedman, P. O., "Erosion of Graphite in Solid Propellant Combustion Gases and Effects on Heat Transfer," *AIAA Journal*, Vol. 3, No. 7, July 1965, pp. 1250–1257.

[3] Kuo, K. K., and Keswani, S. T., "A Comprehensive Theoretical Model for Carbon Carbon Composite Nozzle Recession," *Combustion Science and Technology*, Vol. 42, Nos. 3–4, 1985, pp. 145–164.

[4] Keswani, S. T., Andiroglu, E., Campbell, J. D., and Kuo, K. K., "Recession Behavior of Graphitic Nozzles in Simulated Rocket Motors," *Journal of Spacecraft and Rockets*, Vol. 22, No. 4, July–Aug. 1985, pp. 396–397.

[5] Keswani, S. T., and Kuo, K. K., "Validation of an Aerothermochemical Model for Graphite Nozzle Recession and Heat Transfer Processes," *Combustion Science and Technology*, Vol. 47, Nos. 3–4, 1986, pp. 177–192.

[6] Geisler, R. L., "The Prediction of Graphite Rocket Nozzle Recession Rates," *CPIA publication*, Vol. 342, May 1981, pp. 173–196.

[7] Klager, K., "The Interaction of the Efflux of the Solid Propellants with Nozzle Materials," *Propellants and Explosives*, Vol. 2, June 1977, pp. 55–63.

[8] Patankar, S. V., and Spalding, D. B., *Heat and Mass Transfer in Boundary Layers*, Inter-Text Books, London, 1970.

[9] Launder, B. E., and Spalding, D. B., *Mathematical Models of Turbulence*, Academic Press, New York, 1972.

[10] Gosman, A. D., Lockwood, F. C., and Syed, S. A., "Prediction of Horizontal Free Turbulent Diffusion Flame," *Proceedings of the Sixteenth Symposium (International) on Combustion*, The Combustion Institute, Pittsburgh, 1976, pp. 1543–1555.

[11] Lockwood, F. C., and Naguib, A. S., "The Predictions of Fluctuations in the Properties of Free Round-Jet, Turbulent Diffusion Flames," *Combustion and Flame*, Vol. 24, No. 1, 1975, pp. 109–124.

[12] Libby, P. A., and Blake, T. R., "Burning Carbon Particles in the Presence of Water Vapor," *Combustion and Flame*, Vol. 41, No. 2, 1981, pp. 123–147.

[13] Libby, P. A., "Ignition, Combustion, and Extinction of Carbon Particles," *Combustion and Flame*, Vol. 38, No. 3, 1980, pp. 285–300.

[14] Golovina, E. C., "The Gasification of Carbon by Carbon Dioxide at High Temperatures and Pressures," *Carbon*, Vol. 18, No. 3, 1980, pp. 197–201.

[15] Chelliah, H. K., Makino, A., Kato, I., Araki, N., and Law, C. K., "Modeling of Graphite Oxidation in a Stagnation-Point Flow Field Using Detailed Homogeneous and Semi Global Heterogeneous Mechanisms with Comparisons to Experiments," *Combustion and Flame*, Vol. 104, No. 4, 1996, pp. 469–480.

[16] Chelliah, H. K., "The Influence of Heterogeneous Kinetics and Thermal Radiation on the Oxidation of Graphite Particles," *Combustion and Flame*, Vol. 104, Nos. 1–2, 1996, pp. 81–94.

[17] Rosner, D. E., and Allendorf, H. D., "Comparative Studies of the Attack of Pyrolytic and Isotropic Graphite by Atomic and Molecular Oxygen at High Temperatures," *AIAA Journal*, Vol. 6, No. 4, 1968, pp. 650–654.

[18] Bonnetain, L., and Hoynant, G., *Les Carbones*, edited by A. Pacault, 2, Masson et Cie, Paris, 1965, pp. 270–277.

[19] Neoh, K. D., Howard, J. D., and Sarofim, A. F., "Soot Oxidation in Flames," *Particulate Carbon Formation During Combustion*, edited by D.C. Siegla, and G. W. Smith, Plenum Press, New York, 1981, pp. 162–282.

[20] Nagle, J., and Strickland-Constable, R. F., "Oxidation of Carbon Between 1000–2000 C," *Proceedings of the Fifth Carbon Conference, 1*, Pergamon, Oxford, England, U.K., 1962, pp. 154–164.

[21] Graham, J. A., Brown, A. R. G., Hall, A. R., and Watt, W., "The Rates of Reaction of Carbon and Graphite Materials with Combustion Gases at High Temperatures," *Proceedings of the 1st Conference on Industrial Carbon and Graphite*, Society of Chemical Industry, London, Sept. 1957, p. 309.

[22] Long, F. J., and Sykes, K. W., "The Effect of Specific Catalysts on the Reactions of the Steam-Carbon System," *Proceedings of the Royal Society of London A*, Vol. 215, No. 1120, Nov. 1952, pp. 100–110.

[23] Turkdogan, E. T., Koump, V., Vinters, J. V., and Perzak, T. F., "Rate of Oxidation of Graphite in Carbon Dioxide," *Carbon*, Vol. 6, No. 4, 1968, pp. 467–470.

[24] Turkdogan, E. T., and Vinters, J. V., "Effect of Carbon Monoxide on the Rate of Oxidation of Charcoal, Graphite and Coke in Carbon Dioxide," *Carbon*, Vol. 8, No. 1, 1970, pp. 39–53.

[25] Meyer, L., "The Surface Reaction of Graphite with Oxygen Carbon Dioxide and Water Vapor at Low Pressures," *Transactions of the Faraday Society*, Vol. 34, Feb. 1938, pp. 1056–1061.

[26] Strickland-Constable, R. F., "The Interaction of Carbon Filaments at High Temperatures with Nitrous Oxide, Carbon Dioxide and Water Vapor," *Transactions of the Faraday Society*, Vol. 43, Sept. 1947, pp. 769–778.

[27] Johnstone, J. F., Chen, C. Y., and Scott, D. S., "Kinetics of the Steam-Carbon Reaction in Porous Graphite Tubes," *Industrial and Engineering Chemistry Research*, Vol. 44, No. 7, 1952, p. 1564.

[28] Binford, J. S., Jr., and Eyring, H., "Kinetics of the Steam-Carbon Reaction," *Journal of Physical Chemistry*, Vol. 60, No. 4, 1956, pp. 486–491.

[29] Overholer, L. G., and Brakely, J. P., "Oxidation of Graphite by Low Concentrations of Water Vapor and Carbon Dioxide in Helium," *Carbon*, Vol. 2, No. 4, 1956, pp. 385–394.

[30] Bradley, D., Dixon-Lewis, G., Habik, S. E., and Mushi, E. M. J., "The Oxidation of Graphite Powders in Flame Reaction Zone," *Proceedings of the 20th Symposium (International) on Combustion*, The Combustion Institute, Pittsburgh, 1984, pp. 931–940.

[31] Hurt, R. H., and Haynes, B. S., "On the Origin of Power-Law Kinetics in Carbon Oxidation," *Proceedings of the Thirtieth Symposium (International) on Combustion*, The Combustion Institute, Pittsburgh, 2004, pp. 2161–2168.

[32] Sendt, K., and Haynes, B. S., "Density Functional Study of the Chemisorption of O_2 on the Armchair Surface of Graphite," *Proceedings of the Thirtieth Symposium (International) on Combustion*, The Combustion Institute, Pittsburgh, 2004, pp. 2141–2149.

[33] Freedman, A., "Halogenation of Carbon Surfaces by Atomic Beams: HOPG Graphite," *Diamond and Related Materials*, Vol. 4, No. 3, 1995, pp. 216–219.

[34] Gonzalez, J., Ruiz, M. del C., Bohe, A., and Pasquevich, D., "Oxidation of Carbons in the Presence of Chlorine," *Carbon*, Vol. 37, No. 12, 1999, pp. 1979–1988.

[35] Henning, G., "The Properties of the Interstitial Compounds of Graphite, III. The Electrical Properties of the Halogen Compounds of Graphite," *Journal of Chemical Physics*, Vol. 20, No. 9, Sept. 1952, pp. 1443–1447.

[36] MacDonald, J. A. F., Evans, M. J. B., Liang, S., Meech, S. E., Norman, P. R., and Pears, L., "Chlorine and Oxygen on the Carbon Surface," *Carbon*, Vol. 38, No. 13, 2000, pp. 1825–1830.

[37] Cebeci, T., and Chang, K. C., "Calculations of Incompressible Rough-Wall Boundary Layer Flows," *AIAA Journal*, Vol. 16, No. 7, 1978, pp. 730–735.

[38] Bartz, D. R., "A Simple Equation for Rapid Estimation of Rocket Nozzle Convective Heat Transfer Coefficient," *Journal of Jet Propulsion*, Vol. 37, No. 1, Jan. 1957, pp. 49–51.

[39] Brewster, M. Q., *Thermal Radiative Transfer and Properties*, Wiley, New York, 1992.

[40] El Gorsey, A., and Donnay, G., *Science*, Vol. 161, No. 3839, July 1968, p. 363.

[41] Sladkov, A. M., and Kudryavtsev, Y. P., "Diamond, Graphite, Carbyne —The Allotropic Forms of the Carbon," *Priroda*, Vol. 58, Dec. 1969, pp. 37–44.
[42] Kasatochkin, V. I., Korshak, V. V., Koudrayatsev, Y. P., Sladkov, A. M., and Sterenberg, I. E., *Carbon*, Vol. 11, No. 1, 1973, pp. 70–72.
[43] Nakamizo, M., Kammereck, R., and Walker, P.L., "Laser Raman Studies on Carbons," *Carbon*, Vol. 12, No. 3, 1974, pp. 259–267.
[44] Whittaker, A. G., "Carbon: A New View of its High Temperature Behavior," *Science*, New Series, Vol. 200, No. 4343, 1978, pp. 763–764.
[45] Acharya, R., and Kuo, K. K., "Graphite Rocket Nozzle Erosion Rate Reduction by Boundary-Layer Control Using Ablative Materials," AIAA Paper 2007-0782, 2007.
[46] Wolt, P. J., and Webber, J. A., "Demonstration of a Nozzle Boundary Layer Cooling System (NBLCS) as a Means to Mitigate Nozzle Erosion," *Proceedings of the JANNAF 40th Combustion Subcommittee Meeting*, CPIA, Charleston, SC, 13–17 June 2004.

C. Avedisian
Associate Editor